RESEARCH ARTICLE | JANUARY 15 2025

Temperature and pressure dependence of the fluorescence spectrum of high-pressure synthetic corundum-type $Ga_2O_3:Cr^{3+}$, structural stability, and crystal growth under high pressure

Hitoshi Yusa ✉ ; Masashi Miyakawa

J. Appl. Phys. 137, 035902 (2025)
https://doi.org/10.1063/5.0246260

Journal of Applied Physics ARTICLE pubs.aip.org/aip/jap

Temperature and pressure dependence of the fluorescence spectrum of high-pressure synthetic corundum-type Ga_2O_3:Cr^{3+}, structural stability, and crystal growth under high pressure

Cite as: J. Appl. Phys. **137**, 035902 (2025); doi: 10.1063/5.0246260
Submitted: 31 October 2024 · Accepted: 28 December 2024 ·
Published Online: 15 January 2025

Hitoshi Yusa[a] and Masashi Miyakawa

AFFILIATIONS

Research Center for Materials Nanoarchitectonics, National Institute for Materials Science (NIMS), 1-1 Namiki, Tsukuba, Ibaraki 305-0044, Japan

[a]**Author to whom correspondence should be addressed:** yusa.hitoshi@nims.go.jp

ABSTRACT

The pressure dependence of the R_1 and R_2 peaks of the fluorescence spectra of high-pressure-synthesized corundum-type Ga_2O_3:Cr^{3+} was measured up to 50 GPa using a diamond anvil cell pressurized at room temperature in an argon medium. The temperature dependence of the R_1 and R_2 peaks was measured at low temperatures under ambient pressure from 303 to 83 K. From the measurement results, the pressure scale and low-temperature scale were determined using R_1 and R_2. X-ray diffraction experiments at high pressure, which were performed to confirm the effective range of the pressure scale, showed that the corundum structure undergoes a phase transition to a Rh_2O_3(II)-type structure at 54–65 GPa; this pressure scale is, thus, valid up to approximately 50 GPa. We also investigated the crystal growth time to optimize the crystal size of Ga_2O_3:Cr^{3+} for diamond anvil cell experiments.

I. INTRODUCTION

The ruby fluorescence method is widely used for pressure measurement in diamond anvil cell (DAC) high-pressure devices.[1,2] It is based on the pressure dependence of fluorescence peaks (R_1 and R_2) derived from Cr^{3+} in corundum crystals, and its pressure scale has been determined and updated to higher pressures by various reports.[1,3–8] Instead of Al_2O_3 corundum, we have recently synthesized corundum-type Ga_2O_3 doped with Cr^{3+} at high pressure and have shown that it excites ruby-like fluorescence R_1 and R_2.[9] We reported that not only is the fluorescence intensity stronger than that of ruby, but also light at longer wavelengths than that of ruby fluorescence can be used as the excitation light source. The pressure scale was determined up to 11 GPa at room temperature by measuring its pressure dependence under hydrostatic pressure.[10]

In terms of ionic radius, Ga^{3+} (0.620 Å) is slightly larger than Al^{3+} (0.535 Å) but closer to Cr^{3+} (0.615 Å), making it suitable for allowing Cr^{3+} as a dopant. Interestingly, the fluorescence wavelength at ambient pressure indicates a high-pressure state of ruby of approximately 10 GPa. This may be due to the effect of elemental substitution in the compound on the ligand field of Cr^{3+}: the so-called "chemical pressure" that has been recently proposed.[11] This effect also has a significant impact on the excitation spectrum. Because the excitation spectrum is related to the absorption spectrum, it is very striking that the Ga_2O_3:Cr^{3+} crystal exhibits a green color under white light, which is the opposite of its deep red fluorescent color.[9]

The pressure scale of the ruby fluorescence method has been determined up to approximately 150 GPa.[7,8,12] It deviates from linearity as the pressure increases and is defined by a non-linear equation.[6–8] Therefore, in the present study, we also investigated the pressure dependence of the fluorescence wavelength in corundum-type Ga_2O_3:Cr^{3+} under quasi-hydrostatic conditions at higher pressures and attempted to determine the non-linear form as a pressure scale.

In the case of ruby fluorescence, density functional theory (DFT) calculations report that Al_2O_3 undergoes a structural phase

transition from a corundum type (space group (SG): $R\bar{3}c$) to a Rh_2O_3(II) type (SG: *Pbcn*) above 78–85 GPa:[13–15] in high-pressure experiments, this transition occurs at approximately 95–130 GPa.[16–19] This difference in the pressure values is particularly large at room temperature, where it is not thermally activated. The use of a pressure scale would be limited to the pressure at which the phase transition occurs, but the pressure range would be extended at room temperature, where the corundum structure is maintained in a metastable state. It is also known that Ga_2O_3 undergoes a phase transition to the Rh_2O_3(II) type under high temperature and pressure.[20] In previous research, the phase transition pressure to the Rh_2O_3(II) type at high temperatures was experimentally determined to be approximately 36 GPa at 2000 ± 100 K.[20] This value was consistent with the 30–33 GPa predicted by DFT calculations.[20,21] However, the pressure of the phase transition in the metastable state at room temperature has not been investigated. Therefore, in the present study, we performed *in situ* x-ray diffraction (XRD) experiments on the structural phase transition pressure at room temperature to determine its applicable pressure range as a pressure marker.

There have been many reports on temperature dependence in ruby fluorescence.[22–27] The theoretical background explains that this is caused by a shift in energy level due to the interaction of phonons with the electronic state,[22,25] and the electron–phonon coupling constant has been determined from the temperature dependence of the wavelength shift. In addition, the temperature dependence of the fluorescence spectrum has practical implications in terms of constructing a temperature scale and is also important for clarifying the effects of pressure measurements at low temperatures.[24,28] Therefore, we measured the temperature dependence of the fluorescence spectrum of corundum-type Ga_2O_3:Cr^{3+} crystals below room temperature and compared it with the ruby fluorescence spectrum. We also calculated the electron–phonon coupling constant.

As is often mentioned with respect to ruby fluorescence spectra, differential stresses on the crystal have a significant effect on the peak shape, especially on the R_1 peak shift.[12,29–31] They are caused by uniaxial compression of the crystals in the limited volume of the DAC, such as when the crystals are in contact with the anvil. Therefore, it is recommended that smaller crystals be used. Crushing of the crystals will also affect the internal strain and influence the spectral shape. Rubies can be annealed at high temperatures after pulverization to remove internal strain.[32] However, Ga_2O_3:Cr^{3+} corundum-type crystals cannot be annealed at temperatures higher than 600 °C because their structure reverts to the β-Ga_2O_3 structure.[9] Therefore, synthetic crystals that are small enough not to need crushing are required. It is believed that crystal growth progresses with longer synthesis time, so we evaluated synthesis for different holding times to find the optimal conditions for crystal growth for use as a pressure marker in the DAC.

II. EXPERIMENTAL

Syntheses of corundum-type Ga_2O_3:Cr^{3+} crystals were performed at high temperature and high pressure using a belt-type apparatus (FB30H) at the National Institute for Materials Science (NIMS; Japan).[33] Details of the synthesis method are described in a previous paper.[9] The starting sample was composed of Ga_2O_3 (Kojundo Chemical Laboratory; 99.99% purity) and Cr_2O_3 (Sigma-Aldrich; 99.99% purity) in a molar ratio of 99:1, mixed well in an agate mortar, and dried in a vacuum electric furnace at 130 °C for 3 h. The sample was packed in a gold capsule and placed in a high-pressure cell at 7.7 GPa and 1200 °C for 6, 60, 600 min, or 47 h, then quenched by turning off the heater current, and recovered after decompression. The grain size analysis of the recovered samples was performed for captured images of the crystals under an optical microscope (LEICA Z16 APO) with CCD camera (LEICA Flexacam C3) using ImageJ software.[34]

Structural identification of the synthetic samples by XRD was performed at the Synchrotron Radiation Facility (AichiSR, Japan). Monochromatic x rays (λ = 0.72301 Å) collimated to 100 μm in size were irradiated onto samples fixed in polyimide capillaries. Diffracted x rays were detected with a hybrid pixel array detector (PILATUS 1 M, Dectris, Switzerland). Cooling experiments were performed by blowing nitrogen gas from a refrigerator onto the capillary sample. XRD experiments were performed using the same system operated at room temperature. The temperature was calibrated by diffraction lines from a small amount of gold powder coated on the sample.[35]

The metastability of corundum-type Ga_2O_3:Cr^{3+} structures under high pressure at room temperature was investigated by XRD experiments at the Photon Factory (BL18C and ARNE1), High Energy Accelerator Research Organization (KEK), Japan. A gas membrane was connected to a DAC with anvils of 300 or 250 μm culet size in diameter, and pressure was applied from the rear of the DAC. Experiments were conducted with and without a mixed alcohol pressure media (methanol:ethanol:water = 13:3:1 by volume) to examine the effect of differences in hydrostaticity on phase transition pressure. Monochromatic x rays (50 μm diameter) at a wavelength of 0.62180 and 0.41700 Å were irradiated onto the sample in the DAC, and diffraction lines were detected by a complementary metal–oxide semiconductor (CMOS) flat panel (Teledyne Vison Solutions Rad-icon 2022, USA) detector. The pressure was determined from diffraction lines of Au powder mixed with the sample using an equation of state.[36] All XRD profiles were converted to intensity vs 2θ data using IPAnayzer software.[37] The lattice parameters were refined by profile fitting with PDIndexer software.[37]

The R_1 and R_2 fluorescence spectra at room temperature and high pressure were detected using a spectrometer equipped with a diffraction grating with 1800 grooves/mm and a charge-coupled device detector (CCD; Andor DU401A, USA) with a focal length of 500 mm. A light-emitting diode (LED) laser with a wavelength of 472.8 nm (LASOS, USA) focused at 3 μm diameter was used as the excitation source. Measurements under high pressure were carried out using a DAC with anvils of 300 or 400 μm culet size in diameter. Single crystals of approximately 7 μm in size were placed in a rhenium gasket and sealed in the DAC with an argon pressure medium liquefied with liquid nitrogen. The argon pressure medium would have relatively good quasi-hydrostatic properties at pressures higher than the solidification pressure.[10] Pressure measurements were determined by the pressure dependence of the Raman spectrum of the diamond anvil.[38] These were measured using a separate spectrometer system (Photon Design, Jupiter, Japan) equipped with Ar-ion laser oscillating at 488 nm (Innova, Coherent, USA). To minimize errors due to pressure distribution in the sample chamber, the Raman spectrum of the diamond was

measured directly above the crystal. Spectra at low temperatures were also measured using this spectrometer, and measurements were taken in 10 K increments using a microscope stage with a liquid nitrogen cooling control system that operates at 303 to 83 K (LINCAM THMS600, UK).

III. RESULTS AND DISCUSSION

A. Sample synthesis and crystal growth

The samples synthesized under high pressure were confirmed by XRD to consist of crystals with a corundum-type structure (Fig. S1 in the supplementary material). Micrographs of the synthesized crystals are shown in Figs. 1(a)–1(d). The correlations between synthesis time and averaged, maximum, and minimum grain sizes are shown in Fig. 1(e). The crystals grew in proportion to the synthesis time, indicating that large crystals can be synthesized by keeping the sample in solid-phase reaction for a long time. After about 6 min synthesis time, the average grain size was about 16 μm and many small crystals of less than 10 μm were produced, which were suitable crystal sizes for pressure measurement in the DAC sample chamber. The fluorescence spectra of these crystals were the same as those previously reported for a Cr concentration of 1.0%.[9]

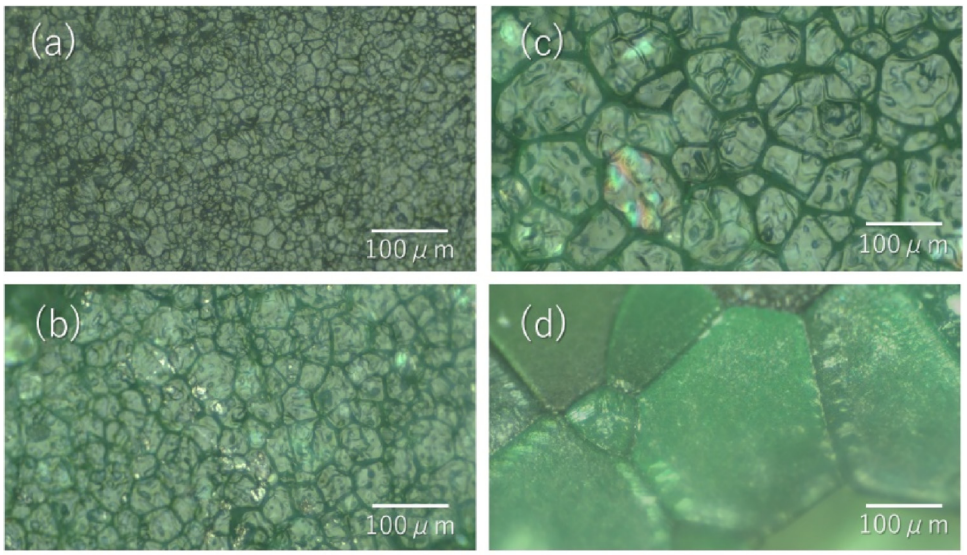

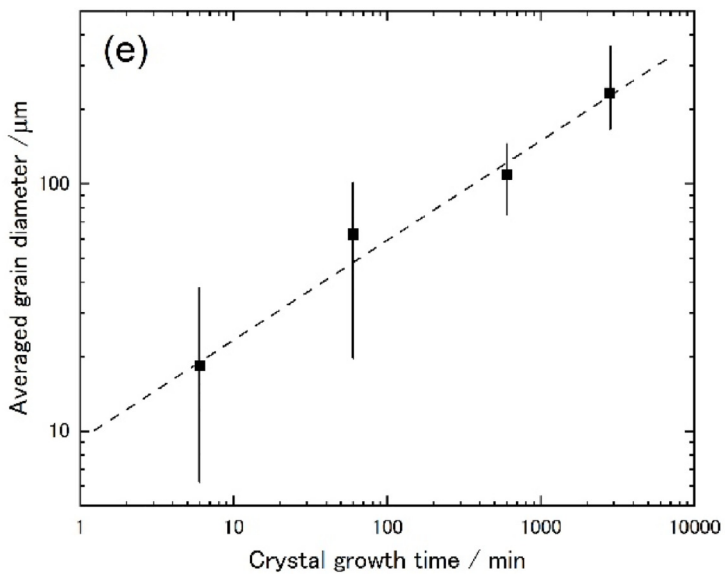

FIG. 1. High-temperature high-pressure-synthesized $Ga_2O_3:Cr^{3+}$ samples. The synthesis times were (a) 6 min, (b) 60 min, and (c) 10, and (d) 47 h. The photograph shows the exposed part after the top of the sample capsule was removed. (e) Particle size distribution.

B. Fluorescence spectra and x-ray diffraction at low temperatures

In the XRD experiments in the low-temperature region down to 84 K, no structural phase transition occurred, and the lattice constant monotonically decreased (Fig. S2 in the supplementary material). The peak wavelengths of the R_1 and R_2 fluorescence shifted to the low-wavelength side as the temperature decreased (Fig. 2). This is the same trend as the fluorescence peaks of ruby, measured in this study and in previous reports,[26] but the shift is considerably larger for Ga_2O_3:Cr^{3+} (1.70 nm) than for ruby (0.95 nm) when cooled from 285 to 84 K. The same trend occurred for the R_2 peak.

According to the theoretical background based on electron–phonon interactions,[25] the wavelength variation with temperature can be described by

$$\nu_0(T) - \nu_0(0) = \alpha(T/\Theta)^4 \int_0^{(\Theta/T)} x^3(e^x - 1)^{-1} dx, \qquad (1)$$

where $\nu_0(T)$ is the wavenumber of R_1 at temperature T at ambient pressure and $\nu_0(0)$ is the wavenumber at 0 K. α and Θ are an electron–phonon coupling parameter and the effective Debye temperature, respectively.

As shown in Fig. 3, fitting the wavenumber data measured for ruby in this study to Eq. (1) yield α and Θ in ruby to be $-453 \pm 13\ cm^{-1}$ and 779 ± 13 K, respectively, which are almost equivalent to the values ($\alpha = -400\ cm^{-1}$ and $\Theta = 760$ K) previously reported.[25] In Ga_2O_3:Cr^{3+}, α and Θ were determined to be $-643 \pm 20\ cm^{-1}$ and 701 ± 13 K, respectively, indicating that the degree of electron–phonon coupling is significantly larger than that in ruby.

In addition to the above-mentioned electron–lattice interactions under isochoric (constant volume) conditions, the cause of the wavelength shift is also related to the thermal expansion of the volume.[2] This can be clarified by examining the change in lattice constants at low temperatures. Figure 4 shows the degree of volume contraction from the standard temperature in comparison with corundum (Al_2O_3).[39,40] The method of deriving the coefficient of thermal expansion using the volume at each measurement temperature is described in the supplementary material, and the linearly approximated values of the coefficient of thermal expansion at each temperature are shown in Fig. S3 in the supplementary material. The coefficient of thermal expansion of Ga_2O_3:Cr^{3+} is larger than that of Al_2O_3. However, the effect of the volume change with temperature on the wavelength shift is about $\Delta\nu = \sim -2.5\ cm^{-1}$

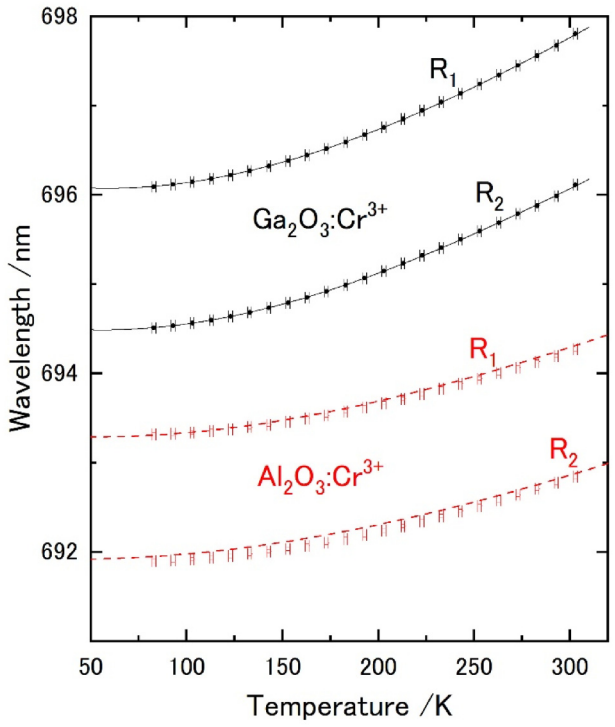

FIG. 2. Temperature dependence of the peak wavelengths of the R_1 and R_2 fluorescence spectra of corundum-type Ga_2O_3:Cr^{3+} and Al_2O_3:Cr^{3+}(ruby). The filled circles and open squares are data from the present measurements, solid lines are the results of fitting using Eqs. (4) and (5), and the broken lines are reported values from Refs. 39 and 40.

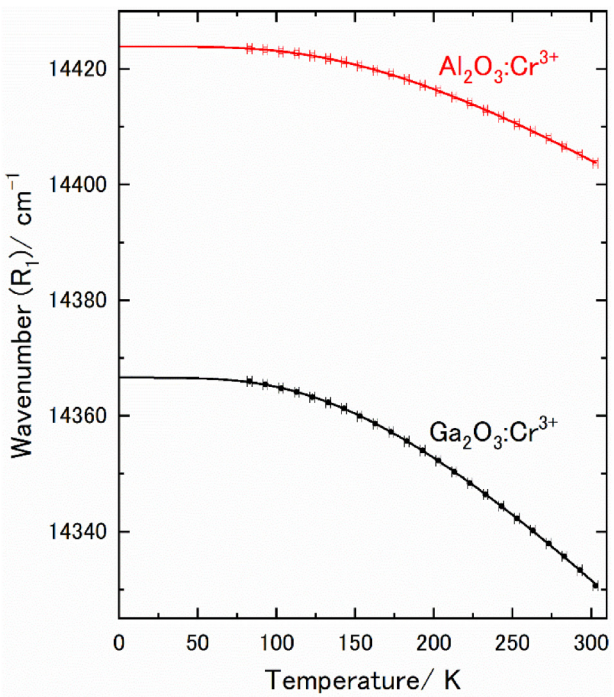

FIG. 3. R_1 fluorescence peak frequencies of corundum-type Ga_2O_3:Cr^{3+} and Al_2O_3:Cr^{3+} as a function of temperature. The lines were obtained by fitting Eq. (1).

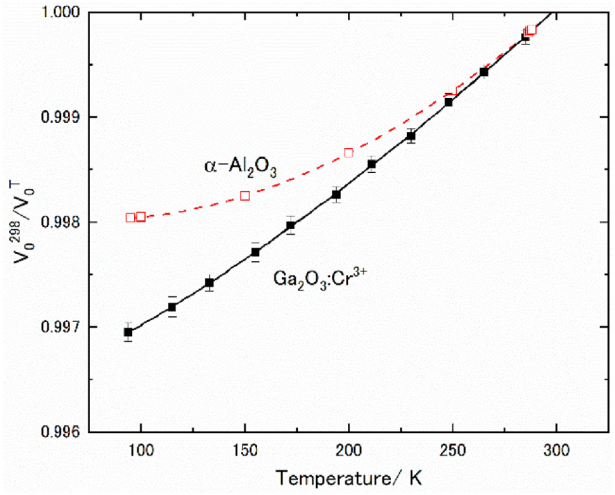

FIG. 4. Volume thermal contraction of $Ga_2O_3:Cr^{3+}$ at low temperatures. Data for corundum (Al_2O_3) are shown for comparison.

($\Delta\lambda \sim +0.12$ nm) per $\Delta T = 100$ K, which is very small compared with the electron–phonon interaction shown in Eq. (1).

From a practical standpoint as a temperature scale, it is helpful to present this as a simple equation. For the wavenumbers, we used the same equation, $R(T) = A_1 + A_2T + A_3T^2 + A_4T^3$, as previously used in the low-temperature measurement of ruby fluorescence.[26] The results for R_1 and R_2 in the measured temperature range were as follows:

$$R_1(T) = 14363 + 10.185 \times 10^{-2}\ T - 9.430 \times 10^{-4}\ T^2 + 8.316 \times 10^{-7}\ T^3 \text{cm}^{-1}, \quad (2)$$

$$R_2(T) = 14396 + 9.346 \times 10^{-2}\ T - 9.047 \times 10^{-4}\ T^2 + 8.595 \times 10^{-7}\ T^3 \text{cm}^{-1}. \quad (3)$$

Similarly, when converted to wavelength and fitted with a third-order polynomial, $R(T) = B_1 + B_2T + B_3T^2 + B_4T^3$, the equations were determined as follows:

$$R_1(T) = 696.211 - 0.493 \times 10^{-2}\ T + 4.558 \times 10^{-5}\ T^2 - 3.987 \times 10^{-8}\ T^3 \text{nm}, \quad (4)$$

$$R_2(T) = 694.607 - 0.450 \times 10^{-2}\ T + 4.356 \times 10^{-5}\ T^2 - 4.113 \times 10^{-8}\ T^3 \text{nm}. \quad (5)$$

The errors in the coefficients of Eqs. (2)–(5) are listed in Table I.

The change in the spectral profile at low temperatures is shown in Fig. 5. As the temperature decreases, it can be seen that R_1 and R_2 can be more clearly separated. Figure 6 shows a plot of full width at half maximum (FWHM) and a comparison with that of ruby. The temperature effect on the FWHM is greater than that of ruby and is reversed below 113 K. Thus, the large temperature dependence and improvement in resolution due to the decrease in the FWHM indicates that $Ga_2O_3:Cr^{3+}$ is a more suitable temperature standard than ruby on the low-temperature side.

TABLE I. Coefficients determined by the regression analysis of Eqs. (2)–(5) and standard error and correlation coefficient (R).

Peak	Coefficient	Values	Standard error	R-square
Eq. (2)				
$R_1(T)$	A_1	14 363	0.582	0.99995
	$A_2 \times 10^2$	10.185	1.034	
	$A_3 \times 10^4$	−9.430	0.488	
	$A_4 \times 10^7$	8.316	0.796	
Eq. (3)				
$R_2(T)$	A_1	14 396	0.675	0.99991
	$A_2 \times 10^2$	9.346	1.201	
	$A_3 \times 10^4$	−9.047	0.584	
	$A_4 \times 10^7$	8.595	0.959	
Eq. (4)				
$R_1(T)$	B_1	696.211	0.028	0.99995
	$B_2 \times 10^2$	−0.493	0.005	
	$B_3 \times 10^5$	4.558	0.237	
	$B_4 \times 10^8$	−3.987	0.386	
Eq. (5)				
$R_2(T)$	B_1	694.607	0.032	0.99991
	$B_2 \times 10^2$	−0.450	0.006	
	$B_3 \times 10^5$	4.356	0.282	
	$B_4 \times 10^8$	−4.113	0.463	

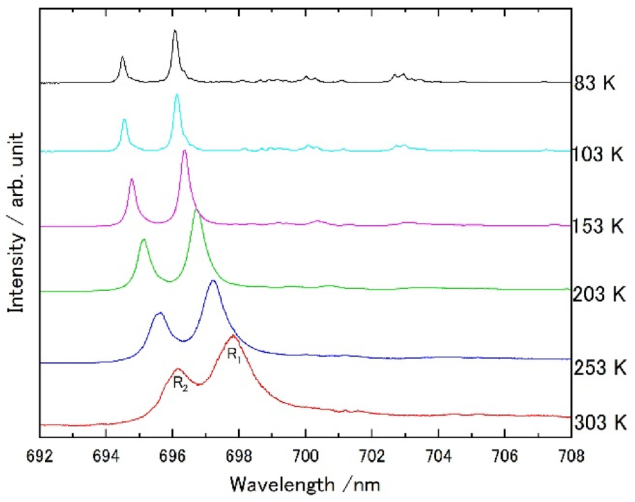

FIG. 5. Typical R_1 and R_2 spectra of $Ga_2O_3:Cr^{3+}$ measured at low temperatures.

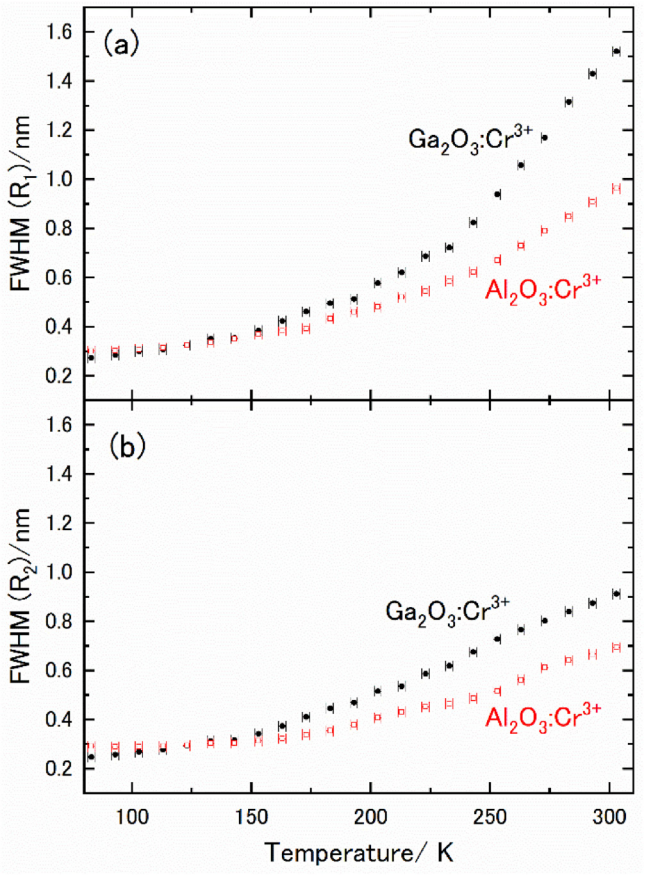

FIG. 6. Temperature dependence of full width at half maximum of the fluorescence spectra of corundum-type $Ga_2O_3:Cr^{3+}$ (filled black circles) and ruby (open squares). (a) and (b) R_1 and R_2, respectively.

C. Pressure dependence of fluorescence spectra and structural stability under high pressure

The pressure scale in the previous paper[9] was determined under fully hydrostatic pressure conditions up to 11 GPa. In the present study, the pressure dependence of the fluorescence spectra was investigated up to higher pressures, with the aim of determining pressure scales up to 50 GPa. For this purpose, the Raman spectrum of the diamond anvil is used for the pressure determination, where the pressure scale equation determined in Akahama and Kawamura[38] is used. This equation is in good agreement with the recently published universal pressure scale by Eremets *et al.*[41] in the pressure range up to 50 GPa. Pressure determination by diamond Raman spectra has one advantage over ruby in the non-hydrostatic regime. Ruby and $Ga_2O_3:Cr^{3+}$ crystals cannot be placed in the same position, and moreover, because of the effect of gasket deformation due to pressurization, the error due to crystal position becomes larger in the pressure region where non-hydrostaticity increases. Therefore, to minimize errors due to pressure distribution in the sample chamber, the Raman spectrum of the diamond was measured directly just above the $Ga_2O_3:Cr^{3+}$ crystal. The results of plotting the peak wavelengths of R_1 and R_2 are shown in Fig. 7(a). These data were fitted to the following non-linear form,[8] which is used as a ruby fluorescence pressure scale, to determine the coefficients and determine the fluorescence pressure

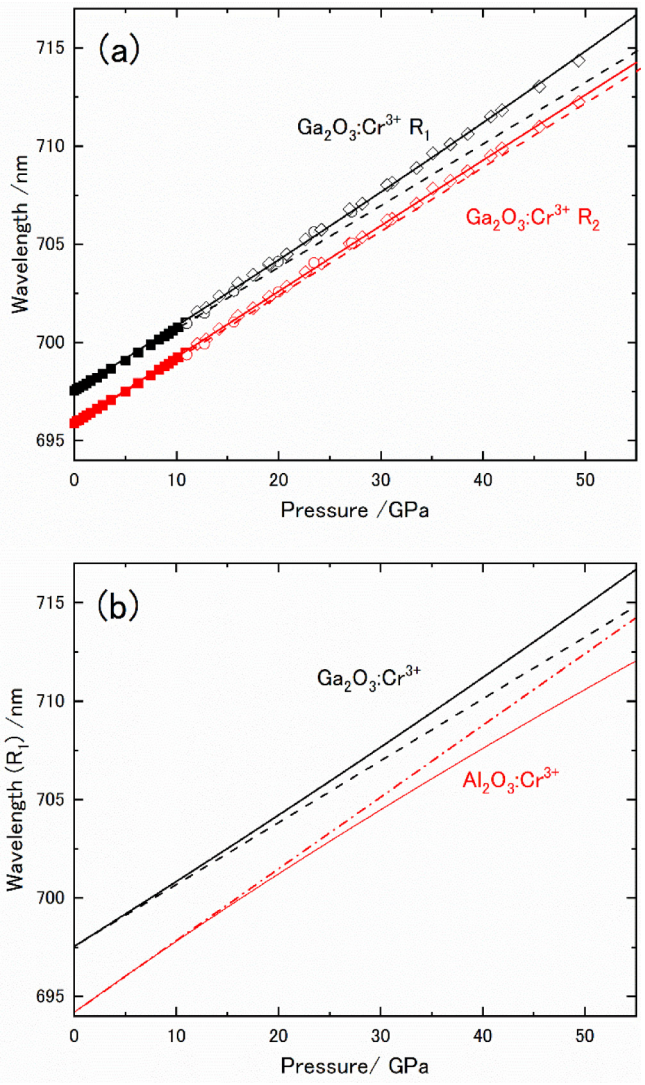

FIG. 7. (a) Pressure dependence of the peak wavelengths of the R_1 and R_2 fluorescence spectra of corundum-type $Ga_2O_3:Cr^{3+}$. The filled squares are from a previous study,[9] which was conducted under hydrostatic conditions with a mixed alcohol pressure media, and the open circles and diamonds are from the present study, which was performed with argon pressure medium. The dashed line is the linear fit of the previous study.[9] (b) Comparison of deviations from the linear pressure scale. The dot-dashed straight line and the thin line show the linear scale[1] and the latest non-linear scale (IPPS-Ruby2020)[8] of ruby, respectively.

TABLE II. Coefficients determined by the regression analysis of Eq. (6) and standard error and correlation coefficient (R).

Peak	Coefficient	Values	Standard error	R-square
$R_1(T)$	A	2.142	0.015	0.99915
	B	−2.340	0.412	
$R_2(T)$	A	2.063	0.013	0.99938
	B	0.345	0.397	

scale,

$$P = A \times 10^3 \left(\frac{\Delta\lambda}{\lambda_0}\right)\left[1 + B\left(\frac{\Delta\lambda}{\lambda_0}\right)\right], \quad (6)$$

where λ_0 are the R_1 and R_2 peak wavelengths at ambient pressure and A and B are the parameters determined by fitting the R_1 and R_2 peak wavelengths. According to the data from this study, $A = 2.142$ and $B = -2.340$ were determined for R_1 and $A = 2.063$ and $B = 0.345$ for R_2. The errors in the coefficients of Eq. (6) are listed in Table II.

The deviation from the linearity of Eq. (6) is shown in Fig. 7(a). The results show that, compared with the pressure scale determined up to 11 GPa, the curve for R_1 shifts upward as the pressure increases and the wavelength pressure dependence becomes slightly larger. Figure 7(b) also shows a deviation from linearity in the pressure scale based on ruby fluorescence, which shows the opposite trend.

In the previous paper,[9] the degree of peak separation was measured under hydrostatic pressure up to 11 GPa and showed a tendency to improve as the pressure increased. The changes in

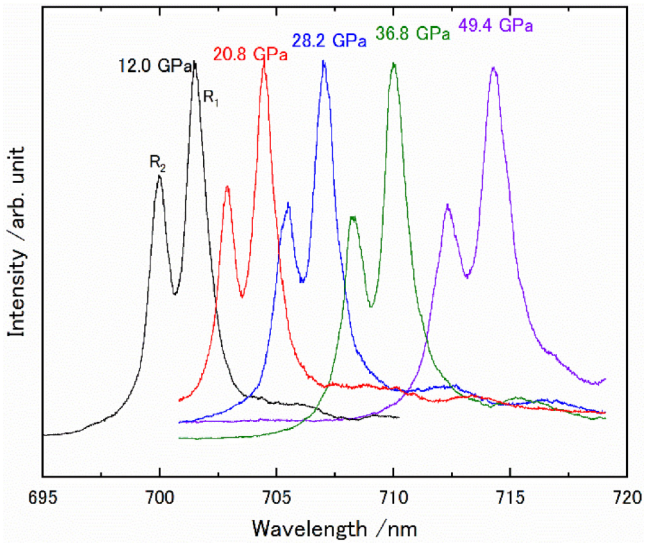

FIG. 8. Typical R_1 and R_2 spectra of $Ga_2O_3:Cr^{3+}$ with increasing pressures.

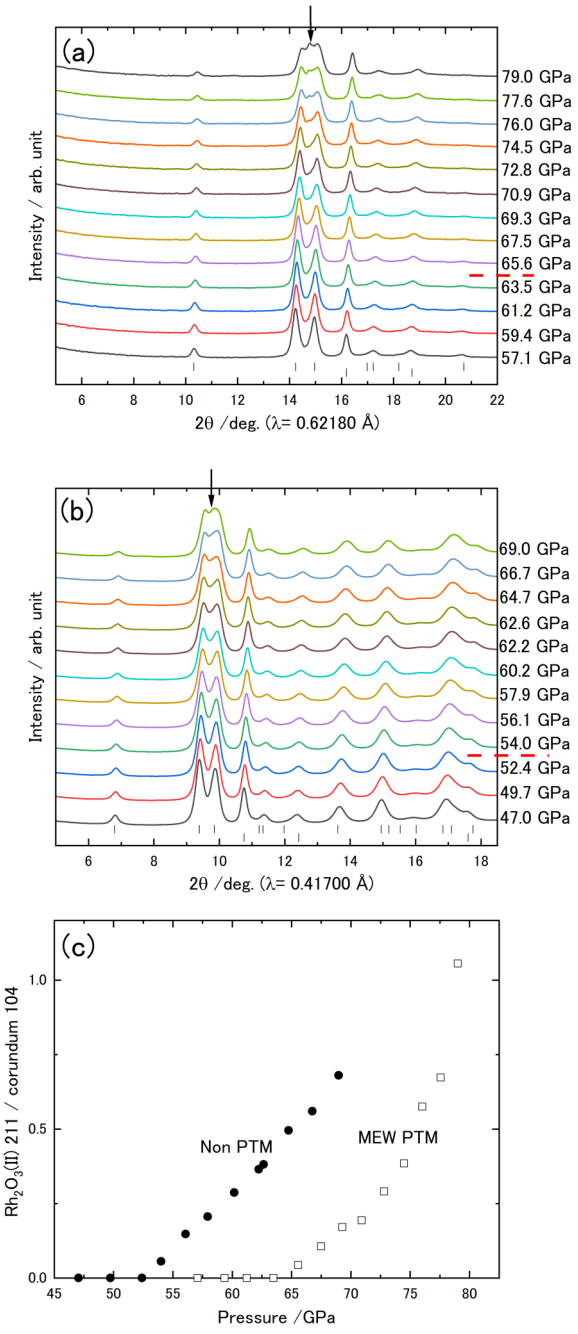

FIG. 9. X-ray diffraction patterns of $Ga_2O_3:Cr^{3+}$ under high pressure (a) using a mixed alcohol medium and (b) without a pressure medium. The bars at the bottom show the position of the diffraction lines representing corundum-type $Ga_2O_3:Cr^{3+}$ (upper) and gold (lower) as a pressure marker. The arrow indicates the 211-diffraction line of the newly appeared $Rh_2O3(II)$ (see the supplementary material). The red broken lines show the estimated transition pressure from corundum to the $Rh_2O_3(II)$ phase. (c) The relative intensity ratio of the $Rh_2O_3(II)$ 211 peak and the corundum 104 peak indicates a degree of conversion from corundum to $Rh_2O_3(II)$.

the fluorescence spectrum up to 50 GPa under quasi-hydrostatic conditions are shown in Fig. 8. The peak separation worsened slightly as the pressure increased due to increasing non-hydrostaticity, but the R_1 and R_2 peaks could still be separated, even at 50 GPa.

To confirm the maximum applicability of this pressure scale, structural changes in Ga_2O_3:Cr^{3+} were investigated by *in situ* XRD experiments. Changes in the diffraction patterns in experiments with and without a mixed alcohol pressure medium are shown in Figs. 9(a) and 9(b), respectively. Both results confirmed that the corundum structure initiates a transition to a Rh_2O_3(II)-type structure, and the phase transition progresses slowly with increasing pressure and is not fully converted in the measured pressure range. The phase transition pressure occurred at 54–65 GPa, depending on the presence of the pressure medium. This difference is similar to the kinetic effect reported for the transition in Al_2O_3, where there is also a large difference between the room-temperature phase transition pressure (109 GPa),[17] the calculated phase transition pressure (78–85 GPa),[13–15] and the phase transition pressure of high-temperature high-pressure experiments (96 GPa).[17–19]

More interestingly, differences in the transition pressure were observed in the present study depending on whether a pressure medium was used or not. When the pressure medium was used, the stability of the corundum structure was ensured up to approximately 65 GPa; the structural phase transition started at approximately 54 GPa in the experimental results obtained under conditions without a pressure medium. The corundum and Rh_2O_3(II)-type structures are linked by a structural relationship of certain twinning-like defects and explained by a displacement-type phase transition.[42] Therefore, this difference may be the effect of non-hydrostaticity promoting a displacement-type phase transition. Thus, we can conclude from these results that the effective range of the pressure-scale equation determined in this study is approximately 50 GPa.

IV. SUMMARY

The pressure dependence of the fluorescence spectrum of Ga_2O_3:Cr^{3+} was measured up to 50 GPa in the argon pressure medium at room temperature, and the pressure scale was determined by fitting with a nonlinear curve equation. The curve shifted upward from linear with increasing pressure. The results of XRD under high pressure at room temperature indicate that the corundum structure is stable up to 54 or 65 GPa, depending on the degree of non-hydrostaticity, and then begins to transition to the Rh_2O_3(II) structure. Therefore, this pressure scale is applicable up to at least 50 GPa. The temperature dependence of the fluorescence wavelength was measured in the range 303–83 K. The temperature dependence was found to be about twice as large as that of ruby, which can be explained by differences in electron–phonon coupling rather than thermal expansion. We investigated the size of crystals produced by changing the synthesis time under high-temperature and high-pressure synthesis conditions at 7.7 GPa and 1200 °C and found that crystals less than 10 μm in size, suitable for DAC experiments, could be grown in 6 min.

SUPPLEMENTARY MATERIAL

See the supplementary material for the XRD profiles of synthesized crystals at different crystal growth times and the calculation of the coefficient of thermal expansion of corundum-type Ga_2O_3:Cr^{3+} and the temperature function formula. All data for the regression analysis of Eqs. (1)–(6) are summarized in Tables SIII–SV, and furthermore, the details of the peak fitting analysis for determining the phase transition of Ga_2O_3:Cr^{3+} from corundum to Rh_2O_3(II) type are summarized. Lattice parameters of Au and pressure values determined by the equation of state in the compression experiment of Ga_2O_3:Cr^{3+} are also given in Table SVI.

ACKNOWLEDGMENTS

This work was supported by JSPS KAKENHI (Grant Nos. 19H05790 and 23K17711) and, in part, by World Premier International Research Center Initiative. The synchrotron radiation experiments were conducted at BL2S1 in AichiSR and BL18C and AR-NE1 in Photon Factory (KEK) with the approval of AichiSR (Proposal Nos. 2023N6005, 2024N1001, and 2024N2002) and KEK (Proposal No. 23G570). Preliminary experiments were conducted at SPring-8 BL10XU (Proposal No. 2023B1344 and 2024A1216). We thank K. Watanabe for his help with spectroscopic measurements under low temperature. We thank Kathryn Sole for editing a draft of this manuscript.

AUTHOR DECLARATIONS

Conflict of Interest

The authors have no conflicts to disclose.

Author Contributions

Hitoshi Yusa: Conceptualization (lead); Data curation (lead); Formal analysis (lead); Funding acquisition (lead); Investigation (lead); Methodology (equal); Project administration (lead); Resources (equal); Supervision (lead); Writing – original draft (lead); Writing – review & editing (equal). **Masashi Miyakawa:** Methodology (equal); Resources (equal); Writing – review & editing (equal).

DATA AVAILABILITY

The data that support the findings of this study are available from the corresponding author upon reasonable request.

REFERENCES

[1]G. J. Piermarini, S. Block, J. D. Barnett, and R. A. Forman, J. Appl. Phys. **46**, 2774 (1975).
[2]K. Syassen, High Pressure Res. **28**, 75 (2008).
[3]H. K. Mao, P. M. Bell, J. W. Shaner, and D. J. Steinberg, J. Appl. Phys. **49**, 3276 (1978).
[4]H. K. Mao, J. Xu, and P. M. Bell, J. Geophys. Res. **91**, 4673 (1986).
[5]W. B. Holzapfel, J. Appl. Phys. **93**, 1813 (2003).
[6]P. I. Dorogokupets and A. R. Oganov, Phys. Rev. B **75**, 024115 (2007).
[7]A. Dewaele, P. Loubeyre, and M. Mezouar, Phys. Rev. B **70**, 094112 (2004).
[8]G. Shen, Y. Wang, A. Dewaele, C. Wu, D. E. Fratanduono, J. Eggert, S. Klotz, K. F. Dziubek, P. Loubeyre, O. V. Fat'yanov, P. D. Asimow, T. Mashimo, and R. M. M. Wentzcovitch, High Pressure Res. **40**, 299 (2020).

[9]H. Yusa and M. Miyakawa, Inorg. Chem. **63**, 2695 (2024).
[10]S. Klotz, J. C. Chervin, P. Munsch, and G. Le Marchand, J. Phys. D: Appl. Phys. **42**, 075413 (2009).
[11]N. Majewska, A. Muñoz, R.-S. Liu, and S. Mahlik, Chem. Mater. **35**, 4680 (2023).
[12]A. Dewaele and P. Loubeyre, High Pressure Res. **27**, 419 (2007).
[13]W. Duan, R. M. Wentzcovitch, and K. T. Thomson, Phys. Rev. B **57**, 10363 (1998).
[14]J. Tsuchiya, T. Tsuchiya, and R. M. Wentzcovitch, Phys. Rev. B **72**, 020103 (2005).
[15]A. R. Oganov and S. Ono, Proc. Natl. Acad. Sci. U.S.A. **102**, 10828 (2005).
[16]N. Funamori and R. Jeanloz, Science **278**, 1109 (1997).
[17]J.-F. Lin, O. Degtyareva, C. T. Prewitt, P. Dera, N. Sata, E. Gregoryanz, H.-k. Mao, and R. J. Hemley, Nat. Mater. **3**, 389 (2004).
[18]J. Kato, K. Hirose, H. Ozawa, and Y. Ohishi, Am. Mineral. **98**, 335 (2013).
[19]W. Shi, W. Wei, N. Sun, Z. Mao, and V. B. Prakapenka, J. Geophys. Res. **127**, 023805, https://doi.org/10.1029/2021JB023805 (2022).
[20]H. Yusa, T. Tsuchiya, N. Sata, and Y. Ohishi, Phys. Rev. B **77**, 064107 (2008).
[21]T. Tsuchiya, H. Yusa, and J. Tsuchiya, Phys. Rev. B **76**, 174108 (2007).
[22]R. C. Powell, B. DiBartolo, B. Birang, and C. S. Naiman, J. Appl. Phys. **37**, 4973 (1966).
[23]I. F. Silvera and R. J. Wijngaarden, Rev. Sci. Instrum. **56**, 121 (1985).
[24]H. Yamaoka, Y. Zekko, I. Jarrige, J.-F. Lin, N. Hiraoka, H. Ishii, K.-D. Tsuei, and J. i. Mizuki, J. Appl. Phys. **112**, 124503 (2012).
[25]D. E. McCumber and M. D. Sturge, J. Appl. Phys. **34**, 1682 (1963).
[26]D. D. Ragan, R. Gustavsen, and D. Schiferl, J. Appl. Phys. **72**, 5539 (1992).
[27]B. A. Weinstein, Rev. Sci. Instrum. **57**, 910 (1986).
[28]K. Nakano, Y. Akahama, Y. Ohishi, and H. Kawamura, Jpn. J. Appl. Phys. **39**, 1249 (2000).
[29]M. Chai and J. Michael Brown, Geophys. Res. Lett. **23**, 3539, (1996).
[30]Y. M. Gupta and X. A. Shen, Appl. Phys. Lett. **58**, 583 (1991).
[31]B. Okai, O. Shimomura, and I. Fujishiro, Physica B+C **139–140**, 799 (1986).
[32]J. C. Chervin, B. Canny, and M. Mancinelli, High Pressure Res. **21**, 305 (2001).
[33]S. Yamaoka, M. Akaishi, H. Kanda, S. Osawa, T. Taniguchi, H. Sei, and O. Fukunaga, J. High Pressure Inst. Jpn. **30**, 249 (1992).
[34]C. A. Schneider, W. S. Rasband, and K. W. Eliceiri, Nat. Methods **9**, 671 (2012).
[35]M. G. Pamato, I. G. Wood, D. P. Dobson, S. A. Hunt, and L. Vočadlo, J. Appl. Crystallogr. **51**, 470 (2018).
[36]T. Tsuchiya, J. Geophys. Res. **108**, 002462, https://doi.org/10.1029/2003JB002446 (2003).
[37]Y. Seto, D. Nishio-Hamane, T. Nagai, and N. Sata, Rev. High Pressure Sci. Technol. **20**, 269 (2010).
[38]Y. Akahama and H. Kawamura, J. Appl. Phys. **100**, 043516 (2006).
[39]Y. V. Shvyd'ko, M. Lucht, E. Gerdau, M. Lerche, E. E. Alp, W. Sturhahn, J. Sutter, and T. S. Toellner, J. Synchrotron Radiat. **9**, 17 (2001).
[40]M. Lucht, M. Lerche, H.-C. Wille, Y. V. Shvyd'ko, H. D. Rüter, E. Gerdau, and P. Becker, J. Appl. Crystallogr. **36**, 1075 (2003).
[41]M. I. Eremets, V. S. Minkov, P. P. Kong, A. P. Drozdov, S. Chariton, and V. B. Prakapenka, Nat. Commun. **14**, 907 (2023).
[42]R. D. Shannon and C. T. Prewitt, J. Solid State Chem. **2**, 134 (1970).